Archimer
http://archimer.ifremer.fr

Reconstructing individual food and growth histories from biogenic carbonates

Laure Pecquerie[a, b, *], Ronan Fablet[c, d], Hélène de Pontual[e], Sylvain Bonhommeau[f], Marianne Alunno-Bruscia[g], Pierre Petitgas[h], Sebastiaan A. L. M Kooijman[i]

[a] University of California Santa Barbara, Department of Ecology, Evolution and Marine Biology, Santa Barbara, Californie 93106-9620, USA
[b] IRD, UMR 212 EME, Centre de Recherche Halieutique Méditerranéenne et Tropicale, 34203 Sète, France
[c] Telecom Bretagne, UMR CNRS 3192 Lab-STICC, 29230 Brest, France
[d] Université Européenne de Bretagne, 35000 Rennes, France
[e] Ifremer, Département Sciences et Technologies Halieutiques, 29280 Plouzané, France
[f] Ifremer, UMR 212 EME, Centre de Recherche Halieutique Méditerranéenne et Tropicale, 34203 Sète, France
[g] Ifremer, Département Physiologie des Organismes Marins, 29840 Argenton-Landunvez, France
[h] Ifremer, Département Ecologie et Modèles pour l'Halieutique, 44300 Nantes, France
[i] Vrije Universiteit, Department of Theoretical Biology, 1081 HV, Amsterdam, The Netherlands

*: Corresponding author : Laure Pecquerie, Tel.: +1 805 893 7115 ; Fax: +1 805 893 8062
email address : laure.pecquerie@lifesci.ucsb.edu

Abstract:

Environmental conditions experienced by aquatic organisms are archived in biogenic carbonates such as fish otoliths, bivalve shells and coral skeletons. These calcified structures present an accretionary growth and variations in optical properties (color or opacity) that are used to reconstruct time. However, full and reliable exploitation of the information extracted from these structures is often limited as the metabolic processes that control their growth and optical properties are poorly understood. Here, we propose a new modeling framework that couples both the growth of a biogenic carbonate and its optical properties with the metabolism of the organism. The model relies on well-tested properties of the Dynamic Energy Budget (DEB) theory. It is applied to otoliths of the Bay of Biscay anchovy *Engraulis encrasicolus*, for which a DEB model has been previously developed. The model reproduces well-known otolith patterns and thus provides us with mechanisms for the metabolic control of otolith size and opacity at the scale of an individual life span. Two original contributions using this framework are demonstrated. (1) The model can be used to reconstruct the temporal variations in the food assimilated by an individual fish. Reconstructing food conditions of past and present aquatic species in their natural environment provides key ecological information that can be used to better understand population dynamics. (2) We show that non-seasonal checks can be discriminated from seasonal checks, which is a well-recognized problem when interpreting fish otoliths. We suggest further developments of the model and outline the experimental settings required to test this new promising framework.

Keywords: Otolith, Calcification, Metabolism, Bioenergetic model, Food re-construction, Dynamic Energy Budget theory.

INTRODUCTION

Calcified structures of aquatic species are remarkable archives of individual life histories and environmental conditions of past and present species. Based on increments that are periodically formed, age, growth, temperature conditions or migrations patterns can be successfully reconstructed (e.g. Quinn *et al.* 1998, Tsukamoto *et al.* 1998, Schone *et al.* 2005). Although δ^{15}N analysis of bulk otolith material is difficult (Elsdon *et al.* 2010), some authors also successfully reconstructed individual trophic position from otolith isotopic composition (Rowell *et al.* 2010). Extracting new information such as temporal variations of assimilated food would represent a remarkable new exploitation of these biogenic carbonates. Knowledge of temporal variations in food conditions could for instance contribute to a better understanding of the dynamics of a population.

A reliable interpretation of these calcified structures relies, however, on our understanding of biomineralization processes and how metabolism and environmental conditions control these processes. In fish and bivalve species, a strong link between carbonate growth and somatic growth has long been demonstrated (Campana 1990, Cerrato 2000). But it is well recognized that growth is not the only metabolic control of carbonate formation. Otolith and shell growth can be decoupled from somatic growth (Campana 1990, Lewis & Cerrato 1997). Slow-growing individuals have somewhat larger otoliths than fast-growing individuals of the same length, which can result in biased back-calculations of growth (Campana 1990). Moreover, a clear link between precipitation rate and metabolic rate has been established in corals (Al-Horani *et al.* 2005), bivalves (Lewis & Cerrato 1997) and fish (Wright *et al.* 2001).

4

The objectives of the present study are twofold. First, we investigate how metabolism controls the formation of biogenic carbonates from a bioenergetic modeling perspective. We explore in particular how starvation events may generate variations in carbonate optical properties and alter the seasonal deposition patterns. Second, we take advantage of the fact that carbonate formation not only depends on somatic growth but on other metabolic processes and aim to demonstrate that not only growth but individual feeding history can be reconstructed from optical properties and growth measurements of biogenic carbonates.

Our new approach benefits from the conceptual and quantitative framework of the Dynamic Energy Budget (DEB) theory for metabolic organization (Kooijman 2010). This general theory describes the uptake and use of energy by an organism according to its environment throughout its life cycle to achieve growth and reproduction. It has been successfully applied to bivalves (e.g. van der Veer *et al.* 2006, Pouvreau *et al.* 2006), fish (e.g. van der Veer *et al.* 2001, Bodiguel *et al.* 2009, Pecquerie *et al.* 2009) and corals (Muller *et al.* 2009) but is applied for the first time to the formation of a specific body part. The conceptual step that leads to a DEB-based model for biogenic carbonates is to consider them as metabolic 'products' (Kooijman 2010). The formation of any 'product' in the context of the DEB theory can potentially be linked to all metabolic functions such as maintenance but also growth and assimilation (Kooijman 2010). Here, as investigated by Hüssy & Mosegaard (2004) for otoliths of juvenile cod, we propose to link both the amount of material that precipitates and its optical properties to the metabolism of the organism. But, in contrast to the former, the present approach is parameter-sparse and simple in view of the number of patterns captured by the model over the lifespan of

5

an individual.

In this paper, we first present the bioenergetic model for biogenic carbonate formation together with the food reconstruction method we developed. The model is then applied to the formation of fish otoliths and is validated by its ability to reproduce known patterns of otolith growth and opacity. Our method for the reconstruction of individual growth and feeding history is then evaluated from model simulations of individuals experiencing different food environments but presenting visually similar otoliths. We finally discuss the potential contributions of our new framework. It first provides a way to better understand the complex interplay between metabolic and environmental controls of biogenic carbonate formation. But it also provides an opportunity to extract new key information from these labor-intensive data: the temporal variations of the food assimilated by individuals throughout their life cycle. We discuss the further model developments and the experimental data required to fully develop and validate this new promising method.

MATERIALS AND METHODS

Standard DEB model   Dynamic Energy Budget (DEB) theory describes the rate at which an organism assimilates and utilizes energy and mass throughout its life cycle as a function of its state and its environment (i.e. food density and temperature) for maintenance, growth, development and reproduction (Fig. 1a; Nisbet *et al.* 2000, Sousa *et al.* 2008, Kooijman 2010). An individual is described by three state variables: the reserve energy E (J), the structural volume V (cm^3) and the reserve energy available for reproduction at the adult stage E_R (J). Stage transitions from embryo to juvenile and juvenile to adult

6

occur at fixed structural volumes: at V_b, the individual starts feeding; at V_p, allocation to maturity is redirected to reproduction (subscripts b and p refer to birth and puberty respectively).

Three energy fluxes determine the dynamics of the state variables: assimilation p_A, growth p_G and dissipation p_D (Fig. 1a). The assimilation process A transforms food into reserve and metabolic products (e.g. faeces and CO_2) (Fig. 1b,c). The growth process G transforms reserve into structure and metabolic products (e.g. CO_2). The dissipation processes D transform reserve into metabolic products (e.g. CO_2) and energy used for maintenance and development processes. Somatic maintenance has priority over growth. In prolonged starvation conditions, i.e. when somatic maintenance costs cannot be covered by reserve energy, an adult can mobilize reserves previously allocated to reproduction (E_R) to cover these somatic maintenance costs (Pouvreau *et al.* 2006, Pecquerie *et al.* 2009). But an individual would die if it is a juvenile, i.e. has no reproduction buffer, or if the reproduction buffer cannot cover somatic maintenance costs. Equations of the model are provided in Table 1 (Eqs. 5-17) ; these equations are given for scaled state variables with no energy dimension (see Pecquerie *et al.* 2009).

[Fig. 1 about here.]

Biogenic carbonate formation Our objective is to link the accretion formation of a biogenic carbonate, i.e. the amount of material that precipitates as well as some optical properties of this material (opacity or color), to the metabolism of an organism. Our main assumption is that biogenic carbonates can be defined as metabolic "products" in the context of the DEB theory

7

138 (Fig. 1d). Like mammal hairs, or tree bark, biogenic carbonates do not require

139 maintenance. Hence they cannot be considered as part of the structural volume

140 V of an individual. They are also not readily available for growth or somatic

141 maintenance and thus cannot be part of the reserve E.

142 We assume that there is no remobilization of material once precipitated. Such

143 remobilization, or dissolution, has only been suggested in extremely stressful

144 conditions in otoliths (Mugiya & Uchimura 1989) and in anaerobic conditions

145 for bivalves (Rhoads & Lutz 1980).

146 Product formation can be expressed as a weighted sum of the three organizing

147 fluxes: assimilation, growth and dissipation (Kooijman 2010). The change in

148 volume $V_{\mathcal{C}}$ of a calcified structure $\mathcal{C}$ is thus given by:

$$149 \qquad \frac{d}{dt} V_{\mathcal{C}} = \frac{1}{\{p_{Am}\}} (v_A p_A + v_G p_G + v_D p_D) \qquad (1)$$

150 with v_i $(i = A, G, D)$ the coefficients (cm d^{-1}) of the assimilation A, growth

151 G and dissipation D contributions. Some of these coefficients can be zero

152 as shown in Fig. 1b for faeces production for instance which is coupled to

153 assimilation only. As in Pecquerie *et al.* (2009), fluxes are scaled by $\{p_{Am}\}$,

154 the maximum surface-area specific assimilation rate, to remove the energy

155 dimension. This scaling reduces the number of parameters to estimate; the

156 flux equations in Table 2 are simplified when scaled by $\{p_{Am}\}$.

157 The contributions from the three organizing fluxes have different chemical

158 compositions (Kooijman 2010) and may therefore contribute differently to the

159 optical properties of the carbonate structure. The contribution of transforma-

160 tion i $(= A, D, G)$ to the opacity (or color) of the *newly* precipitated material

8

O_i is defined by:

$$O_i(t) = \alpha_i \frac{v_i p_i}{\displaystyle\sum_{j=A,D,G} v_j p_j} \tag{2}$$

Constants α_i can be set such that O $(= \sum_i O_i)$ values range between 0 and 1.

We compare the properties of our model with stylized empirical patterns (census Sousa *et al.* 2008), i.e. patterns common to a range of taxa that we assume have similar underlying mechanisms (Table 1). As we apply the model to otolith formation, stylized empirical patterns for otolith formation can also be found in Table 1. Our approach is summarized in Fig. 2. Accordingly, the simulation of individual growth, carbonate growth and opacity as functions of temperature and food is referred as the 'forward' mode (Fig. 2a). The 'backward' mode, described in the following section, refers to the reconstruction of food and carbonate growth from carbonate features (e.g. opacity values along a given transect) (Fig. 2b).

[Fig. 2 about here.]

Reconstructing growth and food conditions The 'backward' mode allows reconstructing the age of an individual, its growth trajectory $L(t)$ and the scaled functional response $f(t)$, using opacity O (or color) measured along a transect $L_{\mathcal{C}}$ of the carbonate structure (Fig. 2). We make the following assumptions: *(i)* the parameters in Table 2 are known (i.e. previously estimated) for a given reference temperature T_1 together with the coefficients v_i $(i = A, D, G)$, *(ii)* the temperature experienced by the individual is known, and *(iii)* the carbonate structure is isomorphic and the relationship between the transect length of the carbonate structure $L_{\mathcal{C}}$ and its volume $V_{\mathcal{C}}$ is known: $V_{\mathcal{C}} = (\delta_{\mathcal{C}} L_{\mathcal{C}})^3$,

9

184 with $\delta_\mathcal{C}$ the carbonate structure shape coefficient.

185 The reconstruction is defined as the determination of the feeding values min-
186 imizing the square deviation between the observed and the predicted opacity
187 (or color) values. This minimization is carried out using a forward gradient-
188 based approach: At each step, given current estimates of the state variables
189 V, the structural volume, and e, the scaled reserve density, at time t_k, we
190 estimate the scaled functional response f_k that minimize the square deviation
191 between predicted and observed $(L_{\mathcal{C}(k+1)}, O_{k+1})$ using Eqs 12, 13, 18 and 19
192 (Table 2). We obtain V_{k+1} and e_{k+1}. This method requires an initialization for
193 V, e and t at the first data point $(L_\mathcal{C}, O)$. This initialization depends on the
194 application and is detailed below for fish otoliths. Given estimated series f, we
195 can deduce the scaled food density $x(t)$ the organism experienced as follows:

$$196 \qquad x(t) = \frac{X(t)}{K} = \frac{f(t)}{1 - f(t)} \tag{3}$$

197 with X the food density and K the saturation constant.

198 All computations for the reconstruction are done with the routine `o2f` in
199 toolbox 'animal' of the software package 'DEBtool' for Octave and Matlab.
200 The package is freely downloadable from
201 `http://www.bio.vu.nl/thb/deb/deblab/`.

202 **Application to fish otoliths** Our model for biogenic carbonates is applied
203 to the formation of a sagitta, the largest otolith among the three otolith pairs
204 located in the inner ear of fish. Our assumption to consider otolith as a product
205 is fully consistent with Wright *et al.* (2001) and Yamamoto *et al.* (1998),
206 who showed a close correlation between otolith growth and O_2 consumption

10

rates (S2,Table 1). DEB theory also implies that, as product formation, O_2 consumption can be expressed as a weighted sum of assimilation, dissipation and growth processes (Kooijman 2010).

We assume that assimilation does not contribute to otolith accretion, i.e. $v_A = 0$ (Eq. 18, Table 2), as short starvation periods do not modify otolith accretion rate (S5, Table 1, Neat *et al.* 2008). Thus, opacity can be expressed as follows:

$$O = \frac{\alpha_G v_G p_G + \alpha_D v_D p_D}{v_G p_G + v_D p_D} \qquad (4)$$

To reproduce translucent bands during slow-growing periods (S8, Table 1), we choose the simplest form of the opacity function, i.e. $\alpha_G = 1$ and $\alpha_D = 0$ (Eq. 19, Table 2). Thus, opacity is decreasing when growth is slowing down and opacity is equal to zero when the individual ceases growth, i.e. when $p_G = 0$. Although choosing such a simple opacity function removes one parameter (α_D), it impedes the reconstruction of the feeding conditions when the individual is not growing (in structure). In this case, i.e. when $p_G = 0$, we can only state that the scaled functional response f is lower than $V^{1/3}/L_m$ (Eq. 13) but we cannot estimate its value. The value $f = V^{1/3}/L_m$ corresponds to the minimum food level required to cover somatic maintenance costs; below this level, we assume that maintenance costs are covered by the reserves previously allocated to reproduction if available (Pouvreau *et al.* 2006, Pecquerie *et al.* 2009). If no reserves are available, the individual dies.

Regarding initialization, a simple approach is to start from a stage transition for which the average length L is documented. Here, we consider the length at the initiation of feeding (referred as birth) L_b (Table 2). If a specific check can be attributed to initiation of feeding in larval otolith (e.g. Rae *et al.* 1999,

11

Lee & Kim 2000), otolith radius at birth $L_{\mathcal{O}b}$ is known. The scaled reserve density at birth e_b is obtained by minimizing the square deviation between the observed and the predicted opacity O_b (Eq. 19, Table 2). The average water temperature at the peak of the spawning period can be taken as the temperature at birth T_b as a first approximation.

Application to the Bay of Biscay anchovy   We apply the model to the Bay of Biscay anchovy (*Engraulis encrasicolus*), which is a small pelagic fish species with a short life-span (4 years). Adult and juvenile data were collected during Ifremer spring acoustic surveys (PEL.2001 to 2005) and autumn survey (JUVESU1999) respectively. Individual data on length (Total Length, TL, nearest 5 mm), age (in days for juveniles, in number of winters for adults, e.g. a Group-1 (G1) individual experienced one winter) and otolith radius (nearest μm) were measured. Data collection and measurement methods are fully described in Petitgas & Grellier (2003) and Allain *et al.* (2003). As anchovy otoliths are observed in reflected light (Cermeño *et al.* 2003, e.g.), translucent bands appear dark in our simulations (Fig. 2).

Parameters of the DEB model for anchovy growth and reproduction (Table 2) are taken from Pecquerie *et al.* (2009). We only need to estimate three new parameters: $\delta_{\mathcal{O}}$, the otolith shape coefficient and v_G and v_D, the coefficients associated with growth and dissipation respectively (Table 2). We need to estimate $\delta_{\mathcal{O}}$ to relate otolith radius (observation) to otolith volume (model variable): $V_{\mathcal{O}} = (\delta_{\mathcal{O}}L_{\mathcal{O}})^3$. We use $W_{\mathcal{O}} = d_{V_{\mathcal{O}}}(\delta_{\mathcal{O}}L_{\mathcal{O}})^3$, with $W_{\mathcal{O}}$ the otolith weight (g), and $d_{V_{\mathcal{O}}} = 2.9$ g cm^{-3} its density (Carlström 1963). For a 12 cm (Standard Length SL) anchovy, which corresponds to a 14 cm (TL) (Wysokinski 1986), Lychakov & Rebane (2005) found $W_{\mathcal{O}} = 0.002402$g. Using the linear

12

relationship we find for adult Bay of Biscay anchovy $L_\mathcal{O} = 0.0402 + 0.0082L$ ($r^2 = 0.77, p < 0.001, n = 3452$), we obtain an average otolith radius $L_\mathcal{O} = 0.155$ cm and a shape coefficient $\delta_\mathcal{O} = 0.6$.

To estimate v_G and v_D, we simulate the body growth and otolith growth of a G3 individual and we minimize the difference between the observed average otolith radius L_O (cm) at a given length L (cm) and the predicted value at the sampling date (June 1$^{\text{st}}$). The same environmental conditions (Fig. 3 a,b) and the same initial conditions at metamorphosis on August 1st ($t = 0$) as in Pecquerie et $al.$ (2009) are used: $L(0) = 4$ cm, $e(0) = f(0)$ and $U_R(0) = 0$ cm^{2}d. The initial otolith radius, i.e. at metamorphosis, $L_\mathcal{O}(0) = 0.06$ cm is obtained from the linear relationship between otolith radius and individual length fitted to juvenile data in the range 3.5 to 4.5 cm ($L_\mathcal{O} = 0.0203L - 0.0239$, $n = 34$, $r^2 = 0.825$, Pecquerie 2008, Fig. 1.10). To compare simulations with observations, we compute the length and the otolith radius of the individual at the sampling date (June 1$^{\text{st}}$). We compare the predicted otolith radius with the average otolith radius observed for fish of the same length using the linear relationship we find for adult Bay of Biscay anchovy mentioned above: $L_O = 0.0402 + 0.0082L$.

[Fig. 3 about here.]

Simulation design In Simulation 1, we study the opacity pattern of an otolith transect from an individual that experienced the seasonal temperature and food conditions used in the parameter estimation procedure (Fig. 3a,b).

In Simulation 2, we compare the observed and predicted average otolith radius of individuals of the same lengths but different ages (G1 and G2, one and two

winters of age, respectively). We expect larger otolith radius in slow-growing individuals (G2) compared to fast-growing individuals (G1) of the same length (e.g. Campana 1990). We simulate the growth of 200 individuals. Individuals randomly hatch between April 1st and August 15th which corresponds to the spawning season of the Bay of Biscay anchovy population (Motos *et al.* 1996). Hatching dates were drawn from a normal distribution with mean June 1st (Julian day 152) and standard deviation 25 days. We use the same seasonal temperature and food conditions as in Simulation 1 but some noise is introduced in each food and temperature trajectory. G1 and G2 individuals are caught at a random date in May, i.e. the period of annual Ifremer surveys. We then compute the average otolith radius per age and size class of these 200 fish.

In Simulation 3, we first investigate the conditions for formation of secondary structures, i.e. translucent bands that are not annual rings (Panfili *et al.* 2002), under starvation conditions ('forward' mode, Fig. 2a). Second, we test the ability of the 'backward' mode to detect such secondary structures and differentiate otoliths with similar patterns. Two individuals are simulated: Individual 1 hatches Year 0 late in the season (July 15th) while Individual 2 hatches earlier in the season (April 1st) the following year (Year 1). Initial conditions are set at the initiation of feeding: $e_b = f$, V_b, $U_{Rb} = 0$ and we set $L_{\mathcal{O}b} = 0.001$ cm for both individuals, which is within the range of otolith radius observed for anchovy larvae at mouth opening(data from Allain *et al.* 2003). The two individuals experience the seasonal temperature conditions used in Simulation 1 (Fig. 3a). While Individual 1 experiences the food conditions used in Simulation 1 (Fig. 3b), Individual 2 experiences better food conditions but a sharp decrease in food conditions before its first winter (Fig. 5g,h). Sampling

14

date is June 1st of Year 3. The 'backward' mode for the reconstruction of feeding history is then applied to both opacity profiles (Fig. 2b) and reconstructed feeding histories are compared with 'experienced' values ('forward' mode, Fig. 2a).

RESULTS

Decoupling between otolith and somatic growth

A 'forward' simulation of the model using realistic average environmental conditions (Figs. 3a,b) reproduces quantitatively well the observed otolith growth patterns of the Bay of Biscay anchovy (Figs. 3c, 4). The simulated individual has a length of $ca.$ 17 cm and an otolith radius of 0.2 cm after three growing periods (Fig. 3c) which is within the range of observed values, 0.16-0.21 cm, for a 17-cm fish (Fig. 4a). However, the predicted otolith radius of small fish are smaller than observed (Fig. 4). The slope of the otolith radius-fish length (OR-FL) relationship is then larger than the observed slope, e.g. 0.011 and 0.008 respectively for G1 individuals. The linear relationship between fish length and otolith radius is nonetheless well reproduced for a large range of anchovy lengths.

Most interestingly, the decoupling between otolith and somatic growth is also quantitatively well reproduced (Fig. 4) although no constraint was added in the parameter estimation procedure to reproduce this observation. This decoupling results in G2 (slow-growing) fish having larger otoliths than G1 (fast-growing) fish of the same length. In the data, 90% of the G1 and the G2 individuals range between 11 and 16 cm and 13 and 18.5 cm, respectively. We

15

thus computed the average otolith radius for each 0.5 cm length class where G1 and G2 individuals are both observed (13-16 cm, Fig. 4a). We find significant differences between average otolith radius of G1 and G2 individuals of the same length in the data (t-tests per length class had p-values $p < 0.01$). The model successfully reproduces the observed difference for each simulated length class (Fig. 4b). Average differences between otolith radius of fish of the same length but different ages are 75 μm in the data and 73 μm in the simulation. The variability in the otolith radius-fish length relationship is, however, lower in our simulation than in the observations as fewer individuals were simulated (Fig. 4b).

[Fig. 4 about here.]

Opacity patterns

The model reproduces alternated opaque and translucent zones (Fig. 3d) as observed opacity patterns in anchovy otoliths (Cermeño *et al.* 2003). One may also notice an overall decrease of the opacity through ontogeny (Fig. 3d) which is commonly observed (Panfili *et al.* 2002).

A particularly interesting feature of the model is its ability to generate secondary structures. In Simulation 3, the two otoliths present three translucent zones and their radii are similar: 2.1 mm and 1.9 mm for Individual 1 and 2, respectively (Fig. 5c,d). These otoliths could both be interpreted as G3 individuals. However, the first translucent zone on the otolith transect of Individual 2 corresponds to a secondary structure (Fig. 5b). This 'check' was generated by stressful feeding conditions (thick arrow in Fig. 5h). During this period,

16

the fish stopped growing for 16 days while some translucent material was still

deposited, which contributed to the growth of the otolith (Fig. 5b,f). It should

be noted that early hatching date in the season associated with greater feeding

conditions for Individual 2 (thin lines, Fig. 5g,h) explain why Individual 1 and

2 have similar otolith sizes despite their difference in age (Fig. 5e,f).

Assimilated food can be quantified from otolith size and opacity

The application of the 'backward mode' to these two individuals is successful

(black lines, Fig. 5e,f): both individual ages and growth patterns are correctly

recovered. We also successfully reconstruct the dynamics of the respective

feeding histories. When growth completely ceases, the reconstruction method

attributes a ceiling value to the assimilated food level (Fig. 5g,h, black lines).

As the individual gets larger, this ceiling value increases: maintenance costs

are proportional to structural volume (Eq. 8) and thus the minimum food

requirements increase as well.

[Fig. 5 about here.]

17

DISCUSSION

In the present work, we developed a modeling tool based on Dynamic Energy Budget (DEB) theory to better understand metabolic control on the formation of biogenic carbonates. We show that the potential of this model is the extraction of new key information from these structures: the food assimilated by individuals in their natural environment. The originality of the approach relies on the assumption that biogenic carbonates can be modeled as metabolic DEB 'products'. Application of this approach to the formation of fish otoliths resulted in a simple model that reproduces known patterns of otolith growth and opacity. The model provides a mechanistic basis for understanding *i)* the decoupling between fish length and otolith radius, *ii)* the overall decrease in opacity as the otolith grows and *iii)* the formation of secondary structures in stressful conditions.

A parameter-sparse model consistent with otolith growth patterns

The resulting bioenergetic model for otolith growth and opacity is a simple model that relies on one key assumption - an otolith is a metabolic 'product' - and three additional parameters, δ_O, v_G and v_D (Table 2) once the bioenergetic model for fish growth and reproduction is calibrated (Pecquerie *et al.* 2009). DEB theory recognizes two compartments (reserve and structure) instead of one (weight) to represent an organism. Some body parts, however, do not follow the definition of structure and reserve: they are not readily available for growth or somatic maintenance (reserve) and do not require maintenance (structure). These body parts can thus be referred as metabolic products,

18

although they are not exchanged with the environment. The formation of these body parts can then be linked to one or more metabolic transformations (Kooijman 2010).

Which transformation contributes to the formation of a specific metabolic product is not prescribed and should be guided by empirical patterns (Table 1). For our otolith application, we assumed that assimilation does not contribute to otolith formation, which simplified greatly the parameter estimation but was not obligatory. This assumption is nonetheless consistent with starvation experiments (Neat *et al.* 2008) and varying feeding frequency experiments (Oyadomari & Auer 2007) that showed no effect on otolith growth and opacity.

By assuming that otolith accretion is coupled not only to somatic growth but also to dissipation processes, the model provides mechanisms for the relationship between somatic growth and otolith accretion. First, the contribution from dissipation processes is small compared to the contribution from growth ($v_G >> v_D$, Table 2). Thus, a tight correlation between otolith radius and fish length, consistent with otolith data (Campana 1990), is obtained despite the fact that no fixed relationship between these quantities is assumed in the model.

Second, the contribution from dissipation processes, though small, explains the well-known decoupling between somatic growth and otolith accretion. The overall contribution of the somatic growth process to the total accretion of the otolith is the same when fish have the same length and does not depend on the time required to reach this length. In contrast, the contribution from dissipation processes is larger in older fish as it is integrated over a longer time period. This results in slow-growing fish having larger otoliths than fast-growing fish

19

of the same length, which is widely observed (Campana 1990). This decoupling is particularly significant for large/old fish during slow-growing periods: *i)* maintenance processes are continuous processes that contribute to otolith accretion even if somatic growth ceases and *ii)* as an individual becomes larger, its maintenance costs increase and so does the contribution from dissipation to otolith accretion.

In our simulation, we obtained smaller than observed otoliths for small fish (Fig.4). By increasing the relative contribution from dissipation compared to growth and assuming that small fish could survive longer in limiting food conditions, we could potentially improve the fit to the data. It requires, however, more detailed work on starvation rules from data that were not available to us.

Metabolism-induced variations in opacity are also consistent with otolith data

By linking opacity to the relative contribution of the growth process, the model reproduces the observations that both juvenile and adult fish develop opaque, high-contrast otoliths during periods of high growth and translucent, low-contrast otoliths during unfavorable growth conditions or starvation (Neilson & Geen 1985, Rice *et al.* 1985). The underlying mechanism in our model is the following: the chemical composition of the contributions from growth and dissipation is different. Therefore, the chemical composition of the material that precipitates varies according to the relative strength of these two processes. Dannevig (1956) showed a link between otolith organic content, consisting of amino acids, and opacity. This observation has since been confirmed and a number of studies showed that translucent structures are dominated by

20

aragonitic calcium crystals, while protein fibers dominate opaque structures (Mugiya 1965, Watabe *et al.* 1982, Hüssy *et al.* 2004). Our model is consistent with the mentioned studies. The contributions from growth and dissipation may, for instance, differ in their protein content, both qualitatively and quantitatively. At this stage, however, we refrain from making this link explicitly for simplicity sake's.

The model also provides mechanisms for both the formation of secondary structures and the overall decrease in opacity as an individual grows. The formation of secondary structures is still poorly understood (Panfili *et al.* 2002) but misinterpretation of such structures lead to age and growth estimation errors (de Pontual *et al.* 2006). Here, in agreement with the assumption formulated by Hoie *et al.* (2008), we show that a severe decrease in food conditions can generate a translucent zone that could be interpreted as a winter ring. Furthermore, as the fish becomes larger, the specific growth rate decreases and the dissipation flux increases due to increased somatic maintenance costs (Eq. 8, Table 2). The decreasing and increasing contributions from growth and dissipation, respectively, to otolith formation result in a decrease in opacity (Eq. 19, Table 2).

The model, however, does not reproduce the decrease in opacity observed in individuals experiencing higher temperatures (Mosegaard & Titus 1987, Otterlei *et al.* 2002, Neat *et al.* 2008). As temperature impacts metabolic processes in the same way in the standard DEB model, the temperature effect on metabolic fluxes currently cancels out in the opacity function (Eq. 19, Table 2). Introducing a temperature-specific effect on $CaCO_3$ precipitation would improve the present model. The precipitation rate of pure aragonite minerals, the normal calcium carbonate polymorph in otoliths, has been shown to increase with

21

temperature (Burton & Walter 1987). Specifying different equations for the organic and the mineral fractions require, however, additional parameters and specific datasets of opacity measurements in different controlled environments which are not currently available for the European anchovy.

Parameter estimation and validation experiments

In this study, we used DEB parameters previously estimated for anchovy (Pecquerie *et al.* 2009). As state variables of the standard DEB model (reserve and structure) are unobservable, estimating DEB parameters for a given species can be challenging. We here refer the reader to a number of studies specifically dedicated to DEB parameter estimation (van der Meer 2006, Kooijman *et al.* 2008, Lika *et al.* 2011) and to a comparison between traditional bioenergetic models and DEB models with a particular emphasis on fish models (Nisbet *et al.* in review). DEB parameters are typically estimated simultaneously by minimizing a weighted sum of squared deviations between a number of datasets and model predictions on feeding, growth, development, and reproduction. The sum of squared deviations is typically weighted depending on the number of data points per dataset and the relevance of the dataset (Lika *et al.* 2011). For fish applications, data such as length-at-age, weight-length relationships and length-fecundity relationships are required (Pecquerie *et al.* 2009, Lika *et al.* 2011). In addition, data on age, length and weight at stage transitions - hatching, first-feeding, metamorphosis, first-reproduction - are particularly useful together with egg descriptors (wet or dry weight, energy content) (Pecquerie *et al.* 2009, Lika *et al.* 2011).

To validate our approach and carefully estimate otolith parameters, opac-

22

ity measurements from controlled experiments are required together with fish length at different points in time. These experiments would ideally be performed over a sufficiently long period to observe variations in growth rates (in length) at the individual scale following variations in food and temperature conditions. As mentioned in the previous section, these data were not available for the European anchovy. Such dataset, however, would be available for cod (*Gadus morhua*) (Hoie *et al.* 2008). Applying our approach to cod requires nonetheless the estimation of cod-specific DEB parameters, which was beyond the scope of the present study. We hope the promising results we obtained will motivate such future work.

Regarding data comparison, the strength of our approach is the possibility to compare a simulated transect and real data in one dimension. To do so, we simulate the total volume of an otolith and assume an isomorphic growth. A single parameter then describes the link between otolith radius and volume. A coupling of our approach with a 2D representation of a biogenic carbonate, as developed by Fablet *et al.* (2009) for otolith, could help resolve situations where the isomorphic growth assumption does not apply, as found for cod (*Gadus morhua*) and whiting (*Merlangius merlangus*) otoliths (Fablet *et al.* 2009) and mussel (*Mytilus edulis*) shell in some conditions (Alunno-Bruscia *et al.* 2001) .

Comparison with other modeling approaches

Compared to other bioenergetic models for otolith formation (Schirripa & Goodyear 1997, Hüssy & Mosegaard 2004), the main difference in our approach is that weight and respiration are not taken as explanatory variables. In a

23

DEB context, growth only refers to the growth in length and not the growth in weight, for instance. Other processes, such as assimilation or reproduction, can be involved in changes in weight. Not differentiating between different metabolic components was presented by Hüssy & Mosegaard (2004) as one of the limitations of their approach. Here, metabolic components that control otolith growth can be differentiated.

Schirripa & Goodyear (1997) suggested that the geometry of the fish body versus the otolith, i.e. the difference between the otolith radius/otolith weight exponent and the fish length/fish weight exponent, was a critical factor in determining the otolith radius (OR)- fish length (FL) relationship and in explaining the decoupling between OR and FL. They emphasized however that backcalculating length with their approach might require the use of different weight-length relationships, e.g. gonad production generate variations in weight that should not be taken into account to backcalculate length. Our approach overcomes this problem and provides a different mechanism for the decoupling between fish length and otolith radius: dissipation processes also contribute to otolith growth.

Our approach also provides a new interpretation of the experiments conducted by Neat *et al.* (2008). These authors suggested that somatic growth and otolith accretion and opacity were not causally related in the short term. A 2-week-starvation experiment on large juvenile cod showed no effect on otolith accretion rate and opacity, although the individuals were losing weight (Neat *et al.* 2008). Reserve acts as a buffer to food variations in our model and the larger the individual, the larger the lag response to food variations. Thus, growth (of structure) continues during short starvation periods in large individuals if they have sufficient reserve. As the loss of reserve is larger than the gain in

24

structure, weight decreases. But as growth and dissipation still occur, otolith growth and opacity may not be significantly affected during these short starvation periods.

Reconstructing growth and food conditions in natural environments

In the present work, we show that our approach can be used to estimate fish age and back-calculate growth in length ('backward' mode) at a much finer scale than the annual pattern. Reconstructing the duration of the non-growing periods (Hüssy & Mosegaard 2004) and detecting secondary structures (de Pontual *et al.* 2006) can be of great value for fisheries research to estimate temporal variability of survival probability for instance or reduce misinterpretations that resulted in biased age and growth estimation.

But we also show that a new key information can potentially be extracted from otolith growth and opacity: the food assimilated by the individual throughout its life span. The energy available to reproduction in natural conditions for instance could in turn be deduced from assimilated food. This method thus can potentially improve the estimation of some demographic parameters and contribute to a better understanding of population dynamics. The specific structure of the model with two state variables to represent biomass and a reserve compartment that buffers food fluctuations in particular are key to reconstruct the feeding history. Without the reserve compartment, we would not be able to reconstruct assimilated food.

Few methods are available to quantitatively characterize feeding in natural conditions over a extended period. In marine mammals and seabirds, stomach

25

temperature recorders have pioneered our ability to document feeding. The magnitude and/or duration of the temperature change in the stomach is assumed to be proportional to the amount of food consumed. Yet, these devices have limitations (e.g. Ropert-Coudert & Kato 2006) and are not available for ectotherms and small organisms in particular. We believe our approach has the potential to overcome these drawbacks. It could also complement Stable Isotope Analysis (SIA) studies, that characterize the qualitative aspects of feeding, in a quantitative way to learn more about temporal resource dynamics and e.g. size-dependent food selection.

In our reconstruction method, we assumed temperature conditions were known. This would require measurements of oxygen isotope ratio $\delta^{18}O$ for instance (e.g. Campana 1999, Quinn *et al.* 1998). It should be noted, however, that our method is not very sensitive to temperature variations experienced by the individual (not shown). Although the data we generated in the forward mode stemmed from a smooth seasonal temperature cycle, we obtained reasonable results using a constant temperature throughout the individual life span in the backward mode.

Although we demonstrate the potential of this approach, it requires validation using opacity measurements in controlled conditions with known food and temperature conditions. Data on cod (*Gadus morhua*) could again be used as otolith data and fish growth data are available from the same experimental settings where group of individuals experience different controlled food and temperature in time and fish growth is measured both in weight and length (e.g. Li *et al.* 2008).

26

Further application of the model: the impact of ocean acidification on biocalcifying organisms

In a context of ocean acidification due to increased levels of atmospheric CO_2, a better understanding of the metabolic control on biogenic carbonates formation could be of great value to distinguish the direct effect of lowered pH on $CaCO_3$ dissolution and an indirect effect on calcification through metabolic responses. Reduced biomineralization of $CaCO_3$ due to lowered pH has been observed in mollusks and corals (e.g. Comeau *et al.* 2009, Cohen *et al.* 2009). Some studies showed no effect of ocean acidification on otolith formation, e.g. in juveniles of the spiny damselfish *Acanthochromis polyacanthus* (Munday *et al.* 2010). However, Checkley *et al.* (2009) and McDonald *et al.* (2009) showed unexpected patterns, i.e. enhanced calcification in otoliths of white sea bass *Atractoscion nobilis* and shell of the barnacle *Amphibalanus amphitrite*, respectively. If one can assume that stressful conditions due to lowered pH increase maintenance processes, our approach suggests that an increase in calcification could be observed. Dissolution processes might, however, counteract this effect and be predominant in numerous species. The approach we developed provides a framework where pH conditions could impact CaCO3 precipitation both directly and indirectly via their impact on metabolic processes. We strongly believe it represents a promising starting point to disentangle and quantify these different impacts of ocean acidification on biogenic carbonate formation and biocalcifying organisms in general.

27

References

Al-Horani FA, Al-Rousan SA, Manasrah RS, Rasheed MY (2005) Coral calcification: Use of radioactive isotopes and metabolic inhibitors to study the interactions with photosynthesis and respiration. Chem Ecol 21: 325–335

Allain G, Petitgas P, Grellier P, Lazure P (2003) The selection process from larval to juvenile stages of anchovy (*Engraulis encrasicolus*) in the Bay of Biscay investigated by Lagrangian simulations and comparative otolith growth. Fish Oceanogr 12: 407–418

Alunno-Bruscia M, Bourget E, Frechette M (2001) Shell allometry and length-mass-density relationship for *Mytilus edulis* in an experimental food-regulated situation. Mar Ecol Prog Ser 219: 177–188

Bodiguel X, Maury O, Mellon-Duval C, Roupsard F, Le Guellec AM, Loizeau V (2009) A dynamic and mechanistic model of PCB bioaccumulation in the European hake (*Merluccius merluccius*). J Sea Res 62: 124–134

Burton EA, Walter LM (1987) Relative precipitation rates of aragonite and Mg calcite from seawater: Temperature or carbonate ion control? Geology 15: 111–114

Campana SE (1990) How reliable are growth back-calculation based on otoliths? Can J Fish Aquat Sci 47: 2219–2227

Campana SE (1999) Chemistry and composition of fish otoliths: pathways, mechanisms and applications. Mar Ecol Prog Ser 188: 263–297

Carlström D (1963) A crystallographic study of vertebrate otoliths. Biol Bull 125: 441–463

Cermeño P, Uriarte A, de Murguia AM, Morales-Nin B (2003) Validation of daily increment formation in otolith of juvenile and adult European anchovy. J Fish Biol 62: 679–691

Cerrato RM (2000) What fish biologists should know about bivalve shells. Fish Res 46: 39–49

Checkley DM, Dickson AG, Takahashi M, Radich JA, Eisenkolb N, Asch R (2009) Elevated CO_2 enhances otolith growth in young fish. Science 324: 1683–1683

Cohen AL, McCorkle DC, de Putron S, Gaetani GA, Rose KA (2009) Morphological and compositional changes in the skeletons of new coral recruits reared in acidified seawater: Insights into the biomineralization response to ocean acidification. Geochem Geophys Geosyst 10: 1–12

Comeau S, Gorsky G, Jeffree R, Teyssie JL, Gattuso JP (2009) Impact of ocean acidification on a key Arctic pelagic mollusc (Limacina helicina). Biogeosciences 6: 1877–1882

Dannevig EH (1956) Chemical composition of the zones in cod otohths. J Cons Int Explor Mer 21: 156–159

de Pontual H, Groison AL, Pineiro C, Bertignac M (2006) Evidence of underestimation of European hake growth in the Bay of Biscay, and its relationship with bias in the agreed method of age estimation. ICES J Mar Sci 63: 1674–1681

Elsdon TS, Ayvazian S, McMahon KW, Thorrold SR (2010) Experimental evaluation of stable isotope fractionation in fish muscle and otoliths. Mar Ecol Prog Ser 408: 195–205

Fablet R, Chessel A, Carbini S, Benzinou A, de Pontual H (2009) Reconstructing individual shape histories of fish otoliths: A new image-based tool for otolith growth analysis and modeling. Fish Res 96: 148–159

Hoff GR, Fuiman LA (1993) Morphometry and composition of red drum otoliths: Changes associated with temperature, somatic growth rate, and age. Comp Biochem Physio A Physio 106: 209–219

Hoie H, Folkvord A, Mosegaard H, Li L, Clausen LAW, Norberg B, Geffen AJ (2008) Restricted fish feeding reduces cod otolith opacity. J Appl Ichthyol 24: 138–143

Hüssy K, Mosegaard H (2004) Atlantic cod (*Gadus morhua*) growth and otolith accretion characteristics modelled in a bioenergetics context. Can J Fish Aquat Sci 61: 1021–1031

Hüssy K, Mosegaard H, Jessen F (2004) Effect of age and temperature on amino acid composition and the content of different protein types of juvenile Atlantic cod (*Gadus morhua*) otoliths. Can J Fish Aquat Sci 61: 1012–1020

Kooijman SALM (2010) Dynamic Energy and Mass Budgets in Biological Systems. 3rd edn. Cambridge University Press, Cambridge

Kooijman SALM, Sousa T, Pecquerie L, van der Meer J, Jager T (2008) From food-dependent statistics to metabolic parameters, a practical guide to the use of dynamic energy budget theory. Biol Rev 83: 533–552

Lee TW, Kim GC (2000) Microstructural growth in otoliths of black rockfish, *Sebastes schlegeli*, from prenatal larval to early juvenile stages. Ichthyol Res 46: 335–341

Lewis DE, Cerrato RM (1997) Growth uncoupling and the relationship between shell growth and metabolism in the soft shell clam *Mya arenaria*. Mar Ecol Prog

Ser 158: 177–189

Li L, Hoie H, Geffen AJ, Heegaard E, Skadal J, Folkvord A (2008) Back-calculation of previous fish size using individually tagged and marked Atlantic cod (*Gadus morhua*). Can J Fish Aquat Sci 65: 2496–2508

Lika K, Freitas V, van der Veer HW, van der Meer J, van der Wijsman JWM, Pecquerie L, Kearney MR, Kooijman SALM (2011) The "covariation method" for estimating the parameters of the standard Dynamic Energy Budget model I: philosophy and approach. Journal of Sea Research (subm.)

Lychakov DV, Rebane YT (2005) Fish otolith mass assymetry: morphometric and influence on acoustic functionality. Hear Res 201: 55–69

McDonald MR, McClintock JB, Amsler CD, Rittschof D, Angus RA, Orihuela B, Lutostanski K (2009) Effects of ocean acidification over the life history of the barnacle *Amphibalanus amphitrite*. Mar Ecol Prog Ser 385: 179–187

Mosegaard H, Titus R (1987) Daily growth rates of otolith yolk sac fry of two salmonids at five different temperatures. *In:* Kullander S O, Fernholm N (eds), *Proceedings of the fifth conference of european ichthylogists* Stockholm: Swedish Museum of Natural History pp. 221–227

Motos L, Uriarte A, Valencia V (1996) The spawning environment of the Bay of Biscay anchovy (*Engraulis encrasicolus* L.) Sci Mar 60: 117–140

Mugiya Y (1965) Calcification of fish and shellfish. X. Study on paper electrophoretic patterns of the acid mucopolysaccharides and Pas-positive materials in the otolith fluid of some fish. Bull Jpn Soc Sci Fish 32: 653–661

Mugiya Y, Uchimura T (1989) Otolith resorption induced by anaerobic stress in the goldfish *Carassius auratus*. J Fish Biol 35: 813–818

Muller E, Kooijman SALM, Edmunds PJ, Doyle FJ, Nisbet RM (2009) Dynamic Energy Budgets in syntrophic symbiotic relationships between heterotrophic hosts and photoautotrophic symbionts. J Theor Biol 259: 44–57

Munday PL, Gagliano M, Donelson JM, Dixson DL, Thorrold SR (2010) Ocean

31

716 acidification does not affect the early life history development of a tropical marine

717 fish. Mar Ecol Prog Ser 423: 211–221

718 Neat FC, Wright PJ, Fryer RJ (2008) Temperature effects on otolith pattern for-

719 mation in Atlantic cod *Gadus morhua*. J Fish Biol 73: 2527–2541

720 Neilson JD, Geen GH (1985) Effects of feeding regimes and diel temperature cy-

721 cles on otolith increment formation in juvenile Chinook salmon, *Oncorhynchus*

722 *tshawytscha*. Fish Bull 83: 91–101

723 Nisbet RM, Muller EB, Lika K, Kooijman SALM (2000) From molecules to ecosys-

724 tems through Dynamic Energy Budget models. J Anim Ecol 69: 913–926

725 Nisbet RM, Jusup M, Klanjscek T, Pecquerie L (in review) Integrating Dynamic

726 Energy Budget (DEB) theory with traditional bioenergetic models. J Exp Biol

727 Otterlei E, Folkvord A, Nyhammer G (2002) Temperature dependent otolith growth

728 of larval and early juvenile Atlantic cod (*Gadus morhua*). ICES J Mar Sci 59:

729 851–860

730 Oyadomari JK, Auer NN (2007) Influence of rearing temperature and feeding regime

731 on otolith increment deposition in larval ciscoes. Trans Am Fish Soc 136: 766–777

732 Panfili J, Troadec H, de Pontual H, Wright PJ (eds) (2002) Manual of Fish Scle-

733 rochronology. Ifremer - IRD coedition, Brest, France

734 Pecquerie L 2008. Bioenergetic modelling of the growth, development and repro-

735 duction of a small pelagic fish: the Bay of Biscay anchovy. Ph.D. thesis Vrije

736 Universiteit, http://dare.ubvu.vu.nl/handle/1871/11716

737 Pecquerie L, Petitgas P, Kooijman SALM (2009) Modeling fish growth and repro-

738 duction in the context of the Dynamic Energy Budget theory to predict environ-

739 mental impact on anchovy spawning duration. J Sea Res 62: 93–105

740 Petitgas P, Grellier P (2003) Size selective processes for anchovy in Biscay, 2000-

741 2002: recruitment, adult survival and spawning. ICES CM 2003/N:07: 11 pp.

742 Pouvreau S, Bourles Y, Lefebvre S, Gangnery A, Alunno-Bruscia M (2006) Appli-

743 cation of a dynamic energy budget model to the Pacific oyster, *Crassostrea gigas*,

32

reared under various environmental conditions. J Sea Res 56: 156–167

Quinn TM, Crowley TJ, Taylor FW, Henin C, Joannot P, Join Y (1998) A multicentury stable isotope record from a New Caledonia coral: Interannual and decadal sea surface temperature variability in the southwest Pacific since 1657 AD. Paleoceanography 13: 412–426

Rae GA, San Romn NA, Spinoglio DE (1999) Age validation and growth of yolked larvae of *Patagonotothen tessellata* (Richardson, 1845) (Pisces: Nototheniidae) from the rocky littoral of the Beagle Channel, Argentina. Sci Mar 63: 469–476

Rhoads DC, Lutz RA (1980) Skeletal growth of aquatic organisms: biological records of environmental change. New York: Plenum Press

Rice JA, Crowder LB, Binkowski FP (1985) Evaluating otolith analysis for bloater *Coregonus hoyi* - Do otoliths ring true? Trans Am Fish Soc 114: 532–539

Ropert-Coudert Y, Kato A (2006) Are stomach temperature recorders a useful tool for determining feeding activity? Polar Biosci 20: 63–72

Rowell K, Dettman D, Dietz R (2010) Nitrogen isotopes in otoliths reconstruct ancient trophic position. Env Biol Fish 89: 415–425

Schirripa MJ, Goodyear CP (1997) Simulation of alternative assumptions of fish otolith-somatic growth with a bioenergetics model. Ecol Model 102: 209–223

Schone BR, Fiebig J, Pfeiffer M, Gless R, Hickson J, Johnson ALA, Dreyer W, Oschmann W (2005) Climate records from a bivalved Methuselah (*Arctica islandica*, Mollusca; Iceland). Palaeogeogr, Palaeoclimateol, Palaeoecol 228: 130–148

Sousa T, Domingos T, Kooijman SALM (2008) From empirical patterns to theory: a formal metabolic theory of life. Phil Trans R Soc Lond B 363: 2453–2464

Tsukamoto K, Nakai I, Tesch WV (1998) Do all freshwater eels migrate? Nature 396: 635–636

van der Meer J (2006) An introduction to Dynamic Energy Budget (DEB) models with special emphasis on parameter estimation. J Sea Res 56: 85–102

van der Veer HW, Kooijman SALM, van der Meer J (2001) Intra- and interspecific

comparison of energy flow in North Atlantic flatfish species by means of dynamic energy budgets. J Sea Res 45: 303–320

van der Veer HW, Cardoso JFMF, van der Meer J (2006) The estimation of DEB parameters for various Northeast Atlantic bivalve species. J Sea Res 56: 107–124

Wanamaker AD, Heinemeier J, Scourse JD, Richardson CA, Butler PG, Eiriksson J, Knudsen KL (2008) Very long-lived mollusks confirm 17th century AD Tephra-based radiocarbon reservoir ages for North Icelandic shelf waters. Radiocarbon 50: 399–412

Watabe N, Tanaka K, Yamada J, Dean JM (1982) Scanning electron microscope observations of the organic matrix in the otolith of the teleost fish *Fundulus heteroclitus* (Linnaeus) and *Tilapia nilotica* (Linnaeus). J Exp Mar Biol Ecol 58: 127–134.

Wright PJ, Fallon-Cousins P, Armstrong JD (2001) The relationship between otolith accretion and resting metabolic rate in juvenile Atlantic salmon during a change in temperature. J Fish Biol 59: 657–666

Wysokinski A (1986) The living marine resources of the Southeast Atlantic. FAO Fish. Tech. Pap. (178) Rev. (1)

Yamamoto T, Ueda H, Higashi S (1998) Correlation among dominance status, metabolic rate and otolith size in masu salmon. J Fish Biol 52: 281–290

Table 1: Stylized facts and empirical evidence on biogenic carbonate formation.

	Stylized facts	Empirical evidence
Biogenic carbonates		
S1	Carbonate growth is strongly correlated to somatic growth	fish: Campana (1990), bivalves: Cerrato (2000)
S2	Carbonate growth is also correlated with metabolic rate	fish: Yamamoto *et al.* (1998), Wright *et al.* (2001), bivalves: Lewis & Cerrato (1997), corals: Al-Horani *et al.* (2005)
S3	Biogenic carbonates form annual rings	fish: Campana (1990), bivalves: Lewis & Cerrato (1997), Wanamaker *et al.* (2008), corals: Quinn *et al.* (1998)
Otoliths		
S4	Slow-growing individuals have larger otoliths than fast-growing fish of the same length	Campana (1990)
S5	Short starvation conditions do not modify otolith accretion rate	Neat *et al.* (2008)
S6	Opacity decreases throughout ontogeny	Hoff & Fuiman (1993)
S7	Opacity increases in colder temperatures	Mosegaard & Titus (1987), Neat *et al.* (2008)
S8	Opacity decreases in poor feeding conditions	Neilson & Geen (1985), Hoie *et al.* (2008)
S9	Secondary structures can be formed	Panfili *et al.* (2002)

Table 2: Variables, parameter values and equations for individual growth, maintenance and reproduction (from Pecquerie *et al.* 2009) and otolith module (this study). Rates are given at the reference temperature $T_1 = 286$ K ($= 13°$C). Calibrated parameters are indicated.

State variables	Unit	Description
$e = (E/V)/[E_m]$		Scaled energy density
V	cm^3	Structural volume
$U_R = E_R/\{p_{Am}\}$	cm^{2}d	Scaled reproduction buffer
V_O	cm^3	Otolith volume
O		Opacity
Link with data		
$L = V^{1/3}/\delta$	cm	Physical length
$L_O = V_O^{1/3}/\delta_O$	cm	Otolith radius
Forcing variables		
x		Scaled food density
T	K	Temperature
$f(x) = x/(x+1)$		Scaled functional response
$c(T) = \exp\left(\frac{T_A}{T_1} - \frac{T_A}{T}\right)$		Temperature correction

Parameters	Value	Unit	Description
T_A	9800	K	Arrhenius temperature
k_M	0.015	d^{-1}	Somatic maintenance rate coefficient (calib.)
g	6		Investment ratio (calib.)
v	0.4	cm d^{-1}	Energy conductance (calib.)
κ	0.65		Allocation to maintenance and growth (calib.)
κ_R	0.95		Allocation to eggs
L_b	0.5	cm	Physical length at birth
L_p	9	cm	Physical length at puberty
δ	0.172		Shape coefficient (calib.)
L_{Vm}	$v/(k_M g)$	cm	Maximum volumetric length
$\{p_{Am}\}$		J cm^{-2}d^{-1}	Maximum surface-area specific assimilation rate
$[E_m]$	$\{p_{Am}\}/v$	J cm^{-3}	Maximum reserve density
δ_O	0.6		Otolith shape coefficient (this study)
v_D	2.37E-04	cm d^{-1}	Coupling coefficient to dissipation (calib., this study)
v_G	3.867E-03	cm d^{-1}	Coupling coefficient to growth (calib., this study)

Equations

$$p_A = c(T)\{p_{Am}\}f(x)V^{2/3} \tag{5}$$

$$p_D = p_M + p_J + (1 - \kappa_R)p_R \tag{6}$$

$$p_G = \kappa p_C - p_M \tag{7}$$

$$p_M = c(T)\frac{\{p_{Am}\}\kappa}{L_{Vm}}V \tag{8}$$

$$p_J = c(T)\frac{\{p_{Am}\}(1 - \kappa)}{L_{Vm}}\min(V, V_p) \tag{9}$$

$$p_R = (1 - \kappa)p_C - p_J \tag{10}$$

$$p_C = c(T)\{p_{Am}\}\frac{eg}{e + g}\left(V^{2/3} + \frac{k_M}{v}V\right) \tag{11}$$

$$\frac{d}{dt}e = c(T)\frac{v}{V^{1/3}}(f(x) - e) \tag{12}$$

$$\frac{d}{dt}V = c(T)\frac{v}{e + g}\left(eV^{2/3} - \frac{V}{L_{Vm}}\right) \tag{13}$$

$$= 0 \quad \text{if starvation (i.e. } e < \frac{V^{1/3}}{L_{Vm}}) \tag{14}$$

$$\frac{d}{dt}U_R = 0 \quad \text{if} \quad V < V_p \tag{15}$$

$$= c(T)(1 - \kappa)\left[\frac{eg}{e + g}\left(V^{2/3} + \frac{k_M}{v}V\right) - \frac{V_p}{L_{Vm}}\right] \text{ if } V \geq V_p \tag{16}$$

$$= c(T)(1 - \kappa)\left[\frac{eg}{e + g}\left(V^{2/3} + \frac{k_M}{v}V\right) - \frac{V_p}{L_{Vm}}\right] - c(T)\frac{\kappa V}{L_{Vm}} \tag{17}$$

$$\text{if starvation}$$

$$\frac{d}{dt}V_O = \frac{1}{\{p_{Am}\}}(v_G p_G + v_D p_D) \tag{18}$$

$$O = \frac{v_G p_G}{v_G p_G + v_D p_D} \tag{19}$$

38

Fig. 1. (a) Energy and mass fluxes in a standard DEB model. The three organizing fluxes are represented: *(i)* assimilation p_A, *(ii)* dissipation p_D = somatic maintenance p_M + maturity maintenance p_J + development p_R and *(iii)* growth p_G. Three examples of metabolic "products" are shown: (b) faeces: contribution from assimilation only, (c) CO_2: contributions from the three transformations and (d) carbonate structure (here an otolith): contributions from growth and dissipation.
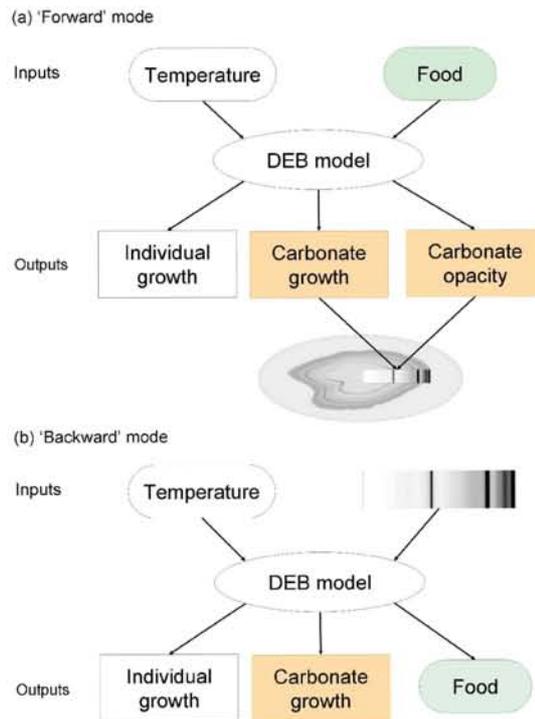
Fig. 2. (a) Approach to model the formation of a biogenic carbonate under metabolic control ('forward' mode). (b) Reconstruction of food conditions, individual and carbonate growth using the features of a biogenic carbonate (radius and opacity) and an average temperature function ('backward' mode).
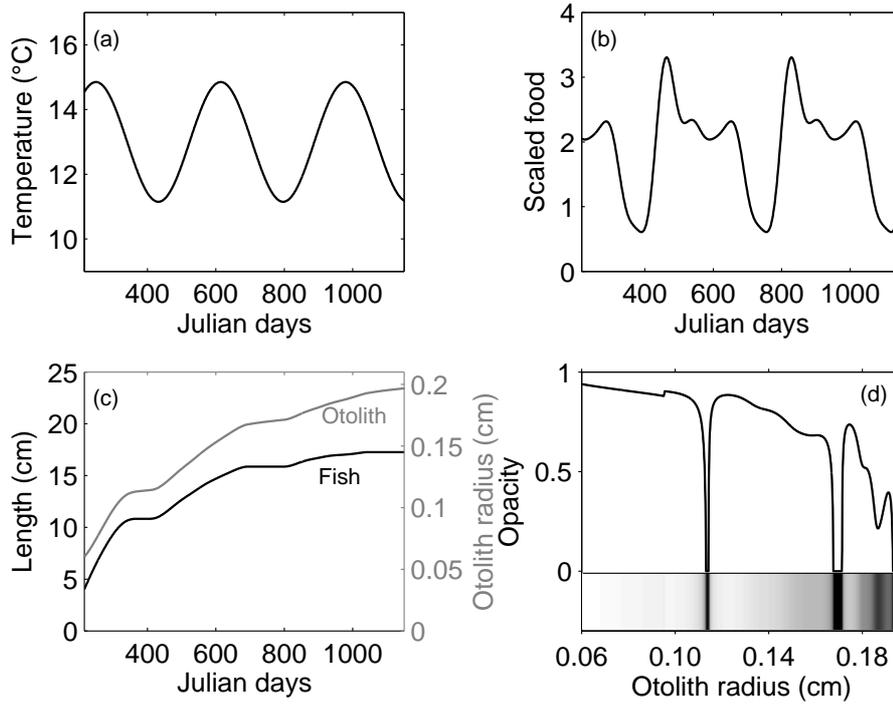
Fig. 3. Simulation of fish growth and otolith formation for a 3-year-old individual that experienced seasonal environment variations (Simulation 1): (a) Temperature, (b) Scaled food density, (c) Fish length (black line) and otolith radius (grey line) as functions of age and (d) Opacity as a function of otolith radius and corresponding image (translucent bands appear dark as if observed in reflected light).

41
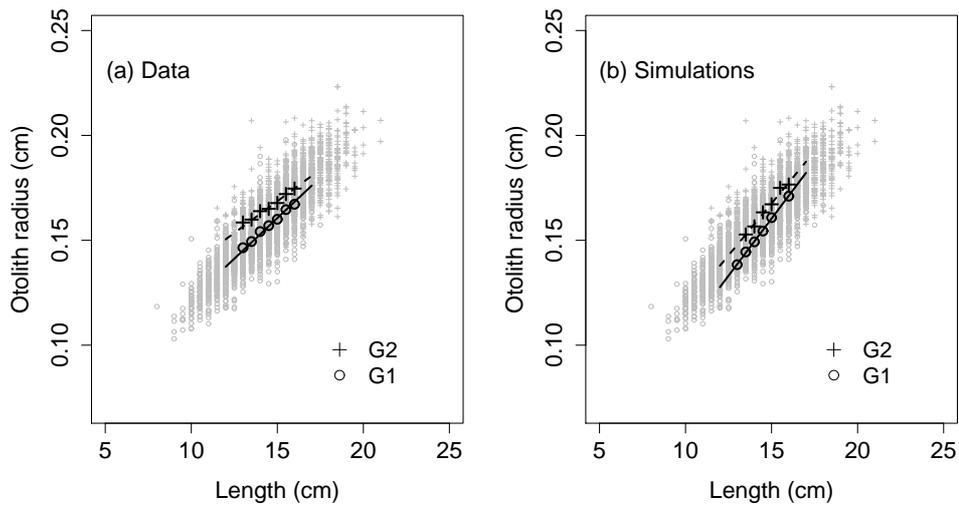
Fig. 4. Average otolith radius (black symbols) per age and fish length class (0.5 cm) for the range 13 - 16 cm (a) in the data for the Bay of Biscay anchovy (*Engraulis encrasicolus*) and (b) in Simulation 2. Grey symbols represent the complete dataset of G1 (=Age 1) and G2 (=Age 2) individuals collected between 2001 and 2005 and are represented in both panels for comparison purposes.
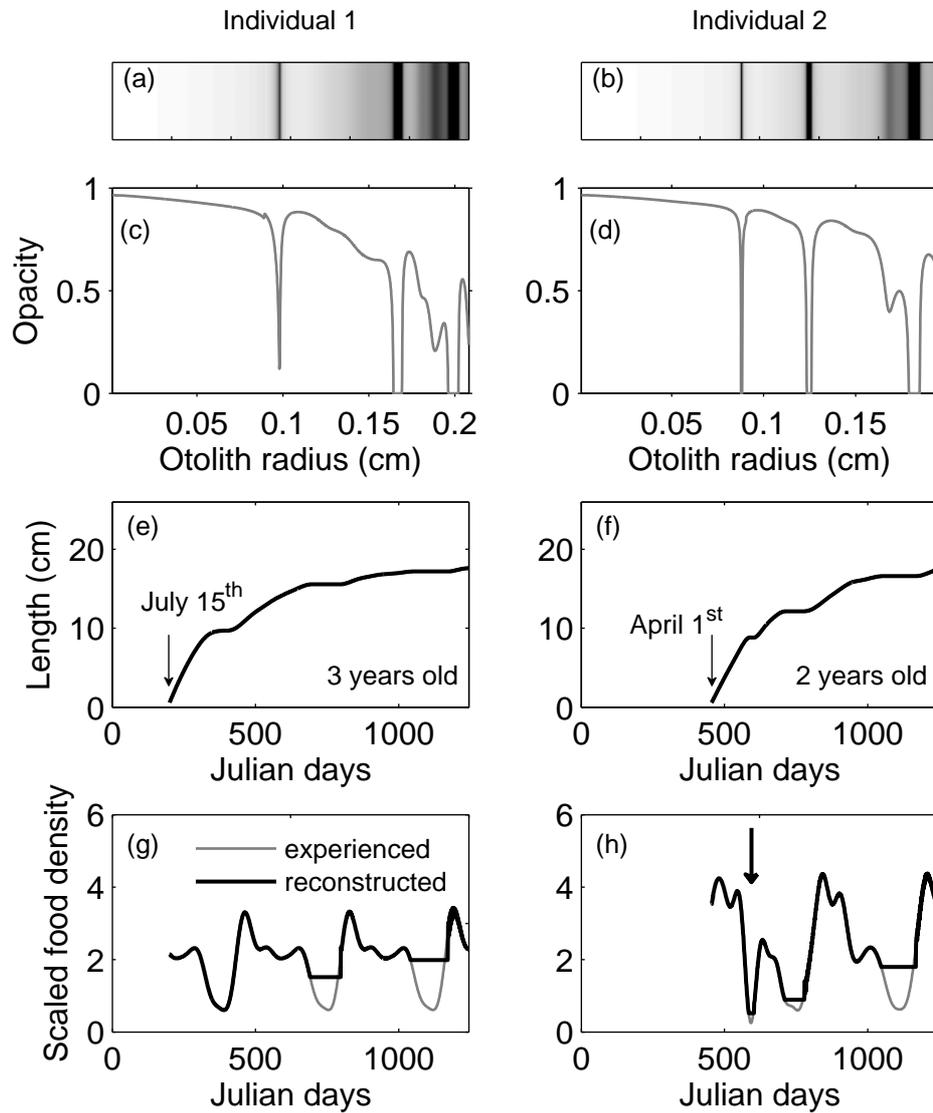
Fig. 5. Reconstruction of growth and scaled food densities experienced by two fish that present translucent zones in their otoliths and that could be both interpreted as G3 fish (Simulation 3). (a, b) Images of the simulated otolith opacity transects for Individual 1 and Individual 2 respectively. (c,d) Corresponding opacity as a function of otolith radius. (e, f) Realized and reconstructed growth: reconstructed growth fully overlapped the realized growth for both individuals. (g, h) Experienced and reconstructed scaled food densities. A thick arrow (h) indicates the starvation period that led to a secondary structure in the otolith of Individual 2.